京都大学
KYOTO UNIVERSITY

KURENAI 紅
Kyoto University Research Information Repository

Abstract

Purpose
This work studies the effect of parameter variations on reduced systems and aims at developing a general formulation for parametrized model order reduction (MOR) methods with the dynamical transition of parameterized state.

Design/methodology/approach
We derive a nonlinear MOR based on the Cauer ladder network (CLN) representation, which serves as an application of the parameterized MOR. Two parametrized CLN representations were developed to handle the nonlinear magnetic field. Simulations using the parameterized CLN were also conducted using an iron-cored inductor model under the first-order approximation.

Findings
Terms including time derivatives of basis vectors appear in nonlinear state equations, in addition to the linear network equations of the CLN method. The terms are newly derived by an exact formulation of the parameterized CLN and are named parameter variation terms in this study. According to the simulation results, the parameter variation terms play a significant role in the nonlinear state equations when reluctivity is used, while they can be neglected when differential reluctivity is used.

Practical implication
The computational time of nonlinear transient analyses can be greatly reduced by applying the parameterized CLN when the number of time steps is large.

Originality
We introduced a general representation for the dynamical behavior of the reduced system with time-varying parameters, which has not been theoretically discussed in previous studies. The effect of the parameter variations is numerically given as a form of parameter variation terms by the exact derivation of the nonlinear state equations. The influence of parameter variation terms was confirmed by simulation.

Keywords: Model order reduction, eddy currents, magnetic saturation.

Article Type: Research paper

Model Order Reduction of Nonlinear Eddy-current Field Using Parameterized CLN

Miwa Tobita[1], Hamed Eskandari[1], and Tetsuji Matsuo[1]
[1] Graduate School of Engineering, Kyoto University, Kyoto 6158510, Japan

1. INTRODUCTION

The coupled analysis of an electric machine and its control circuit requires efficient computation of the electromagnetic field. In recent years, several model order reduction (MOR) methods have been developed to provide reduced systems, wherein the number of unknown variables for electromagnetic field representations is reduced without the loss of accuracy. To handle the reduced systems under multiple states, some MOR methods have parameterized representation depending on the degree of magnetic saturation (Sato *et al.,* 2017; Hasan *et al.,* 2018; Eskandari and Matsuo, 2020), temperature, and the rotational angle of the motors (Henneron and Clenet, 2014; Shimotani *et al.*, 2016). The dynamical behavior of such reduced systems, however, has not been rigorously discussed with time-varying orthogonal basis functions. A short article by Tobita and Matsuo (2020) derived the exact state equations of reduced systems, including the variation of the basis functions.

In this work, we numerically study the effect of the parameter variation on reduced systems and aim to develop a general formulation for parametrized MOR methods with the dynamical transition. We further derive a nonlinear MOR based on the Cauer ladder network (CLN) representation, which serves as an application of the parameterized MOR. The CLN method (Kameari *et al.,* 2018; Matsuo *et al.,* 2018) is a procedure that reduces the electromagnetic field distribution provided by the finite element method (FEM) to Cauer network representation. The method retains a clear physical meaning in the form of the Cauer network with the help of the orthogonal function expansion, which is a significant advantage over other MORs. In this study, two parameterized CLN representations are developed for handling the nonlinear magnetic field: one parameterizes reluctivity, and the other parameterizes differential reluctivity to reflect the degree of saturation.

2. CLN METHOD BASED ON RELUCTIVITY

2.1 Parameterized CLN

The eddy-current field in the finite element space is represented by

$$Ka = \sigma e, \tag{1}$$

$$Ce = -\frac{\mathrm{d}}{\mathrm{d}t}Ca, \tag{2}$$

where C is the edge-face incident matrix, and e and a are variable vectors of the electric field and magnetic vector potential, respectively. The reluctivity matrix v and conductivity matrix σ are defined as follows:

$$v = \{v_{ij}\}, \; v_{ij} = \int_{\Omega} \frac{1}{\mu} w_i^2 \cdot w_j^2 \mathrm{d}\Omega, \tag{3}$$

$$\sigma = \{\sigma_{ij}\}, \; \sigma_{ij} = \int_{\Omega} \sigma w_i^1 \cdot w_j^1 \mathrm{d}\Omega, \tag{4}$$

where Ω is the analysis domain, w_i^1 and w_i^2 are finite element basis functions, μ is the permeability, and σ is the conductivity.

The CLN procedure with a fixed reluctivity matrix v generates basis vectors e_{2n} and a_{2n+1}, and network elements R_{2n} and L_{2n+1} ($n = 0, 1,...$) (Matsuo *et al.,* 2018) as

$$K(a_{2n+1} - a_{2n-1}) = R_{2n}\sigma e_{2n}, \tag{5}$$

$$e_{2n+2} - e_{2n} = -\frac{1}{L_{2n+1}}a_{2n+1}, \tag{6}$$

$$1/R_{2n} = e_{2n}^{\mathrm{T}}\sigma e_{2n}, \; L_{2n+1} = a_{2n+1}^{\mathrm{T}}Ka_{2n+1}, \tag{7}$$

where $K = C^{\mathrm{T}}vC$ is the stiffness matrix, and $a_{-1} = 0$. The basis vectors satisfy orthogonal relations

$$e_{2i}^{\mathrm{T}}\sigma e_{2j} = \delta_{ij}/R_{2i}, \; a_{2i+1}^{\mathrm{T}}Ka_{2j+1} = \delta_{ij}L_{2i+1}, \tag{8}$$

where δ_{ij} is the Kronecker delta.

We assume that the variable vectors a and e are expanded as follows:

$$a = \sum_n I_{2n+1}a_{2n+1}, \tag{9}$$

$$e = \sum_n V_{2n}e_{2n}. \tag{10}$$

Substituting equations (9) and (10) into (1) and (2), we obtain

$$K\sum_n I_{2n+1}a_{2n+1} = \sigma\sum_n V_{2n}e_{2n}, \tag{11}$$

$$C\sum_n V_{2n}e_{2n} = C\sum_n V_{2n}e_{2n} - CV_S e_0$$
$$= -\frac{\mathrm{d}}{\mathrm{d}t}\sum_n I_{2n+1}Ca_{2n+1}, \tag{12}$$

where the initial condition is given by an electrostatic field e_0, which satisfies $Ce_0 = 0$, and V_S is the source voltage. Equation (12) yields

$$\sum_n V_{2n}e_{2n} - V_S e_0 = -\frac{\mathrm{d}}{\mathrm{d}t}\sum_n I_{2n+1}a_{2n+1}. \tag{13}$$

In this study, it is assumed that the reluctivity matrix v is parameterized by the degree of magnetic saturation. Because v depends on the magnetic flux density $\sum_n I_{2n+1}Ca_{2n+1}$, it can be considered a function of α in the parameterized CLN as follows:

$$v = v(\alpha), \; \alpha = (I_1, I_3, ...). \tag{14}$$

Assuming that the first mode current I_1 has a huge impact on the saturation, we approximate it as a function of I_1 by choosing $\alpha = I_1$, which was also referred to as the first-

order approximation in the study by Eskandari and Matsuo (2020). Thus, we have

$$\boldsymbol{v} = \boldsymbol{v}\,(\alpha),\ \alpha = I_1. \tag{15}$$

Figure 1 shows a general form of the parameterized CLN, wherein the circuit elements derived using $\boldsymbol{v}\,(\alpha)$ are functions of α.
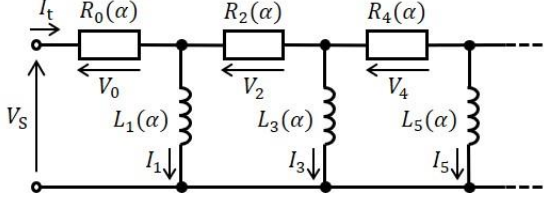

Figure 1. CLN parametrized with α.

2.2 Exact Derivation of Nonlinear State Equations

Multiplying $\boldsymbol{a}_{2k+1}/L_{2k+1}$ to both sides of equation (11) and using equations (6) and (8), we obtain

$$I_{2k+1} = \frac{V_{2k}}{R_{2k}} - \frac{V_{2k+2}}{R_{2k+2}} \quad (k = 0, 1, \ldots). \tag{16}$$

Multiplying $R_{2k}\boldsymbol{\sigma}\boldsymbol{e}_{2k}$ to both sides of equation (13) and using equation (5), we obtain

$$R_{2k}\boldsymbol{e}_{2k}^{\mathrm{T}}\boldsymbol{\sigma}\left(\sum_n V_{2n}\boldsymbol{e}_{2n} - V_S\boldsymbol{e}_0\right)$$
$$= -\left(\boldsymbol{a}_{2k+1} - \boldsymbol{a}_{2k-1}\right)^{\mathrm{T}}\boldsymbol{K}\frac{\mathrm{d}}{\mathrm{d}t}\sum_n I_{2n+1}\boldsymbol{a}_{2n+1}. \tag{17}$$

Using equations (8) and (15), equation (17) can be rewritten as

$$V_{2k} = L_{2k-1}\frac{\mathrm{d}I_{2k-1}}{\mathrm{d}t} - L_{2k+1}\frac{\mathrm{d}I_{2k+1}}{\mathrm{d}t}$$
$$- \left(\boldsymbol{a}_{2k+1} - \boldsymbol{a}_{2k-1}\right)^{\mathrm{T}}\boldsymbol{K}\sum_n I_{2n+1}\frac{\mathrm{d}\boldsymbol{a}_{2n+1}}{\mathrm{d}\alpha}\frac{\mathrm{d}\alpha}{\mathrm{d}t}$$
$$(k = 1, 2, \ldots), (18)$$

$$V_0 = V_S - L_1\frac{\mathrm{d}I_1}{\mathrm{d}t} - \boldsymbol{a}_1^{\mathrm{T}}\boldsymbol{K}\sum_n I_{2n+1}\frac{\mathrm{d}\boldsymbol{a}_{2n+1}}{\mathrm{d}\alpha}\frac{\mathrm{d}\alpha}{\mathrm{d}t}. \tag{19}$$

The last terms in equations (18) and (19) concerning $\mathrm{d}\boldsymbol{a}_{2n+1}/\mathrm{d}\alpha$ are called parameter variation terms. These terms appear because of the variation of the system parameters and were newly derived by the exact formulation of the parameterized CLN, which has been conducted above. When $\alpha = I_1$, the term that includes $\mathrm{d}\boldsymbol{a}_{2n+1}/\mathrm{d}I_1$ can be prepared before solving the network equations.

Under the circumstances that the parameter variation terms are negligible, equations (18) and (19) are approximated as

$$V_{2k} = L_{2k-1}\frac{\mathrm{d}I_{2k-1}}{\mathrm{d}t} - L_{2k+1}\frac{\mathrm{d}I_{2k+1}}{\mathrm{d}t} \quad (k = 1, 2, \ldots), \tag{20}$$

$$V_0 = V_S - L_1\frac{\mathrm{d}I_1}{\mathrm{d}t}. \tag{21}$$

Equations (16), (20), and (21) correspond to the Cauer network equations with constant reluctivity (Matsuo *et al.*, 2018).

3. CLN METHOD BASED ON DIFFERENTIAL RELUCTIVITY

3.1 Parameterized CLN

When a differential reluctivity is used instead of

reluctivity, equations (1) and (2) can be rewritten as

$$\boldsymbol{C}^{\mathrm{T}}\boldsymbol{h} = \boldsymbol{\sigma}\boldsymbol{e}, \tag{22}$$

$$\boldsymbol{C}\boldsymbol{e} = -\left(\boldsymbol{v}^d\right)^{-1}\frac{\mathrm{d}\boldsymbol{h}}{\mathrm{d}t}, \tag{23}$$

where $\boldsymbol{h}$ is the variable vector of the magnetic field. The differential reluctivity matrix $\boldsymbol{v}^d$ is defined by

$$\boldsymbol{v}^d = \{v_{ij}^d\},\ v_{ij}^d = \int_\Omega \boldsymbol{w}_i^2 \cdot \left(\frac{\partial \boldsymbol{H}}{\partial \boldsymbol{B}}\boldsymbol{w}_j^2\right)\mathrm{d}\Omega, \tag{24}$$

where $\partial\boldsymbol{H}/\partial\boldsymbol{B}$ is a second-order tensor of the differential reluctivity.

The CLN procedure with the differential reluctivity matrix $\boldsymbol{v}^d$ for a fixed α consists of the following equations:

$$\boldsymbol{K}^d\left(\boldsymbol{a}_{2n+1}^d - \boldsymbol{a}_{2n-1}^d\right) = R_{2n}^d\boldsymbol{\sigma}\boldsymbol{e}_{2n}^d, \tag{25}$$

$$\boldsymbol{e}_{2n+2}^d - \boldsymbol{e}_{2n}^d = -\frac{1}{L_{2n+1}^d}\boldsymbol{a}_{2n+1}^d, \tag{26}$$

$$1/R_{2n}^d = \left(\boldsymbol{e}_{2n}^d\right)^{\mathrm{T}}\boldsymbol{\sigma}\boldsymbol{e}_{2n}^d,\ L_{2n+1}^d = \left(\boldsymbol{a}_{2n+1}^d\right)^{\mathrm{T}}\boldsymbol{K}^d\boldsymbol{a}_{2n+1}^d, \tag{27}$$

The basis vectors, the network elements, and the stiffness matrix are denoted by superscript d, because they are different from those with reluctivity v.

Similar to the case with the reluctivity v, the basis vectors satisfy orthogonal relations

$$\left(\boldsymbol{e}_{2i}^d\right)^{\mathrm{T}}\boldsymbol{\sigma}\boldsymbol{e}_{2j}^d = \delta_{ij}/R_{2i}^d,\ \left(\boldsymbol{a}_{2i+1}^d\right)^{\mathrm{T}}\boldsymbol{K}^d\boldsymbol{a}_{2j+1}^d = \delta_{ij}L_{2i+1}^d. \tag{28}$$

We assume vectors $\boldsymbol{h}$ and $\boldsymbol{e}$ are expanded as follows:

$$\boldsymbol{h} = \sum_n I_{2n+1}\boldsymbol{v}^d\boldsymbol{C}\boldsymbol{a}_{2n+1}^d, \tag{29}$$

$$\boldsymbol{e} = \sum_n V_{2n}\boldsymbol{e}_{2n}^d. \tag{30}$$

Substituting equations (29) and (30) into (22) and (23), we obtain

$$\boldsymbol{K}^d\sum_n I_{2n+1}\boldsymbol{a}_{2n+1}^d = \boldsymbol{\sigma}\sum_n V_{2n}\boldsymbol{e}_{2n}^d, \tag{31}$$

$$\boldsymbol{K}^d\sum_n V_{2n}\boldsymbol{e}_{2n}^d = -\frac{\mathrm{d}}{\mathrm{d}t}\left(\sum_n I_{2n+1}\boldsymbol{K}^d\boldsymbol{a}_{2n+1}^d\right). \tag{32}$$

The reluctivity matrix $\boldsymbol{v}^d$ is parameterized by the degree of saturation as follows.

$$\boldsymbol{v}^d = \boldsymbol{v}^d\,(\alpha),\ \alpha = I_1. \tag{33}$$

3.2 Exact Derivation of Nonlinear State Equations

From equations (26), (28), and (31), we have

$$I_{2k+1} = \frac{V_{2k}}{R_{2k}^d} - \frac{V_{2k+2}}{R_{2k+2}^d} \quad (k = 0, 1, \ldots). \tag{34}$$

Transforming equation (32) and taking the initial conditions into account, we obtain

$$\boldsymbol{K}^d\left(\sum_n V_{2n}\boldsymbol{e}_{2n}^d - V_S\boldsymbol{e}_0^d\right) = -\boldsymbol{K}^d\sum_n \boldsymbol{a}_{2n+1}^d\frac{\mathrm{d}I_{2n+1}}{\mathrm{d}t}$$
$$- \sum_n I_{2n+1}\frac{\mathrm{d}\left(\boldsymbol{K}^d\boldsymbol{a}_{2n+1}^d\right)}{\mathrm{d}t}. \tag{35}$$

Multiplying $\left(\boldsymbol{a}_{2k+1}^d - \boldsymbol{a}_{2k-1}^d\right)$ to both sides of equation (35) and using equations (25) and (28), we obtain the following equations:

$$V_{2k} = L_{2k-1}^d\frac{\mathrm{d}I_{2k-1}}{\mathrm{d}t} - L_{2k+1}^d\frac{\mathrm{d}I_{2k+1}}{\mathrm{d}t}$$

$$-\left(\boldsymbol{a}_{2k+1}^{d}-\boldsymbol{a}_{2k-1}^{d}\right)^{\mathrm{T}}\sum_{n}I_{2n+1}\frac{\mathrm{d}\left(\boldsymbol{K}^{d}\boldsymbol{a}_{2n+1}^{d}\right)}{\mathrm{d}\alpha}\frac{\mathrm{d}\alpha}{\mathrm{d}t}$$
$$(k=1,2,\dots),\ (36)$$

$$V_{0}=V_{S}-L_{1}^{d}\frac{\mathrm{d}I_{1}}{\mathrm{d}t}-\left(\boldsymbol{a}_{1}^{d}\right)^{\mathrm{T}}\sum_{n}I_{2n+1}\frac{\mathrm{d}\left(\boldsymbol{K}^{d}\boldsymbol{a}_{2n+1}^{d}\right)}{\mathrm{d}\alpha}\frac{\mathrm{d}\alpha}{\mathrm{d}t}\ .\ (37)$$

The last terms in equations (36) and (37) concerning $\mathrm{d}\left(\boldsymbol{K}^{d}\boldsymbol{a}_{2n+1}^{d}\right)/\mathrm{d}\alpha$ are the parameter variation terms. They can be prepared before the computation of time evolution when $\alpha=I_{1}$.

If the parameter variation terms are negligible, equations (36) and (37) are approximated as

$$V_{2k}=L_{2k-1}^{d}\frac{\mathrm{d}I_{2k-1}}{\mathrm{d}t}-L_{2k+1}^{d}\frac{\mathrm{d}I_{2k+1}}{\mathrm{d}t}\quad(k=1,2,\dots),\ (38)$$

$$V_{0}=V_{S}-L_{1}^{d}\frac{\mathrm{d}I_{1}}{\mathrm{d}t}.\tag{39}$$

Equations (34), (38), and (39) correspond to the nonlinear Cauer network equations examined by Eskandari and Matsuo (2020).

4. RESULTS OF COMPUTATIONS

The two-dimensional iron-cored inductor, shown in figure 2, was analyzed. Only a quarter of the whole domain was calculated by the utilization of its line symmetry. We assumed that the iron core consists of bulk material. The magnetic characteristics of the iron core are represented by the polynomial function

$$\boldsymbol{H}=v_{i}\left[h_{1}\left(\frac{|\boldsymbol{B}|}{B_{0}}\right)^{a}+h_{2}\right]\boldsymbol{B},\tag{40}$$

where $v_{i}=(1/4\pi)\times10^{3}$ m/H, $h_{1}=2$, $h_{2}=1$, $B_{0}=1$ T, and $a=6$.

The B–H characteristics of the iron core, represented by equation (40), are shown in figure 3. The conductivity of the iron core is 1.0×10^{6} S/m, while the reluctivity and conductivity of the coil are $(1/4\pi)\times10^{7}$ m/H and 4.0×10^{6} S/m, respectively.
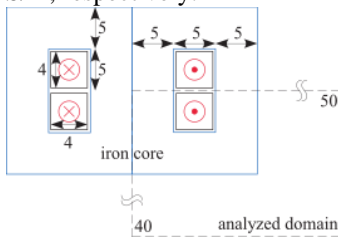
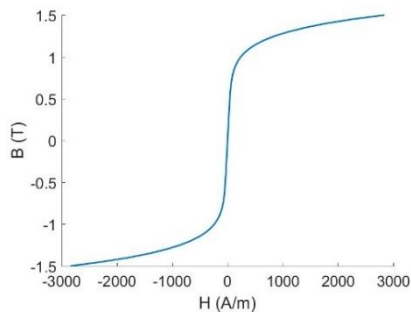**Figure 2.** Iron-cored inductor with dimensions in millimeters.

Figure 3. B–H characteristics of the iron core assumed in the simulation.

4.1 Preparation of Network Elements and Parameter Variation Terms

The network elements R, L, R^{d}, and L^{d} are calculated along with several parameter variation terms before solving the state equations. They are obtained for $\alpha=I_{1}=$ 0–200 A with intervals of 0.1, 1, and 10 A for $0\le I_{1}\le10$ A, $10<I_{1}\le100$ A, and $I_{1}>100$ A, respectively.

Figure 4 shows the variations in R_{2n} and L_{2n+1} ($n=0,1,2$) based on the reluctivity v for $I_{1}=0$–50 A. The inductance of L_{2n+1} decreases as I_{1} increases owing to magnetic saturation. L_{1} is larger than L_{2n+1} ($n>1$).

The variations of R_{2n}^{d} and L_{2n+1}^{d} ($n=0,1,2$) based on the differential reluctivity v^{d} are shown in figure 5 for $I_{1}=$ 0–50 A. Tendencies similar to those of R_{2n} and L_{2n+1} are observed, except for the slope of L_{2n+1}^{d} against I_{1}, which is steeper than that of L_{2n+1}.
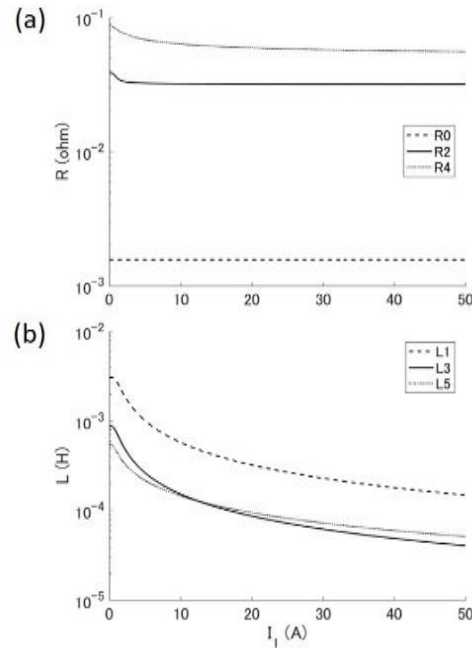
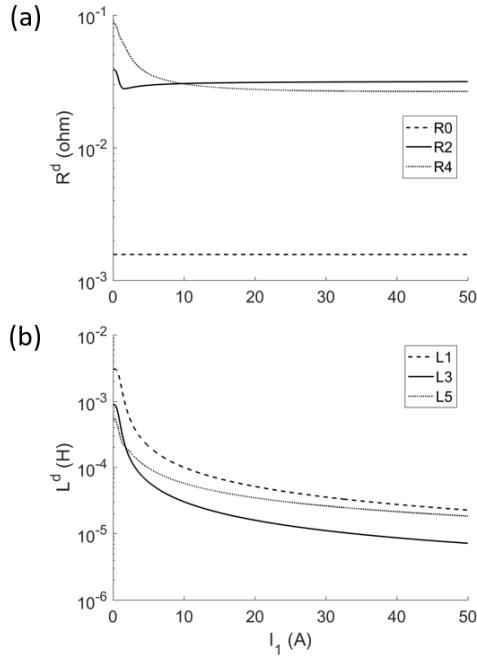**Figure 4.** Result of (a) R_{2n} and (b) L_{2n+1} using v.

Figure 5. Result of (a) R_{2n}^d and (b) L_{2n+1}^d using v^d.

A part of the parameter variation terms can be prepared beforehand. The $\mathrm{d}\boldsymbol{a}_{2n-1}/\mathrm{d}I_1$ part in the parameter variation terms is obtained by calculating the central difference of $\boldsymbol{a}_{2n-1}$ regarding I_1. The results of $\boldsymbol{a}_{2k-1}^{\mathrm{T}}\boldsymbol{K}\mathrm{d}\boldsymbol{a}_{2n-1}/\mathrm{d}I_1$ are shown in figure 6 for $(k, n) = (1, 1)$, $(1, 3)$, $(3, 1)$, and $(3, 3)$. The dominance of component $(k, n) = (1, 1)$ is clearly observed. The components with $k \neq n$ were small. In particular, $(k, n) = (3, 1)$ remains almost zero for all I_1.

When the differential reluctivity v^d is used, $\left(\boldsymbol{a}_{2k-1}^d\right)^{\mathrm{T}} \mathrm{d}\left(\boldsymbol{K}^d \boldsymbol{a}_{2n-1}^d\right)/\mathrm{d}I_1$ is prepared by the central difference scheme regarding I_1, as shown in figure 7 for $(k, n) = (1, 1)$, $(1, 3)$, $(3, 1)$, and $(3, 3)$. Unlike the result based on the reluctivity v, the component $(k, n) = (1, 1)$ is small, whereas the $(k, n) = (3, 1)$ term is dominant.
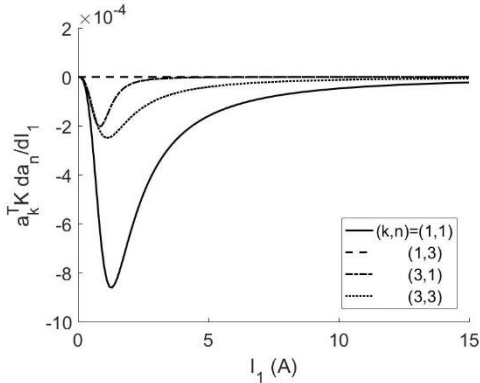

Figure 6. Result of $\boldsymbol{a}_{2k-1}^{\mathrm{T}}\boldsymbol{K}\mathrm{d}\boldsymbol{a}_{2n-1}/\mathrm{d}I_1$ using v.
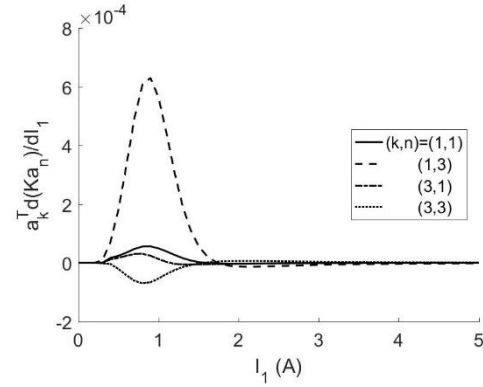
Figure 7. Result of $\left(\boldsymbol{a}_{2k-1}^d\right)^{\mathrm{T}} \mathrm{d}\left(\boldsymbol{K}^d \boldsymbol{a}_{2n-1}^d\right)/\mathrm{d}I_1$ using v^d.

By combining the results in figures 4 and 6, we obtain $L_1 + I_1 \boldsymbol{a}_1^{\mathrm{T}}\boldsymbol{K}\mathrm{d}\boldsymbol{a}_1/\mathrm{d}I_1$, which is represented by the solid line in figure 8, and L_1 is also shown in this figure for comparison. As I_1 increases, the solid line moves farther away from the dashed line, which indicates that the parameter variation terms have a significant influence on the inductance.

The corresponding result based on differential reluctivity v^d is shown in figure 9. The term $L_1^d + I_1 \left(\boldsymbol{a}_1^d\right)^{\mathrm{T}} \mathrm{d}\left(\boldsymbol{K}^d \boldsymbol{a}_1^d\right)/\mathrm{d}I_1$ is represented by the solid line, which is almost identical to the dashed line showing L_1^d. The influence of the parameter variation term was expected to be negligible.
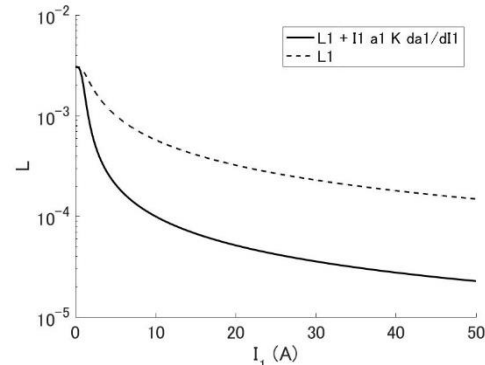

Figure 8. Result of $L_1 + I_1 \boldsymbol{a}_1^{\mathrm{T}}\boldsymbol{K}\mathrm{d}\boldsymbol{a}_1/\mathrm{d}I_1$ using v is plotted in solid line.
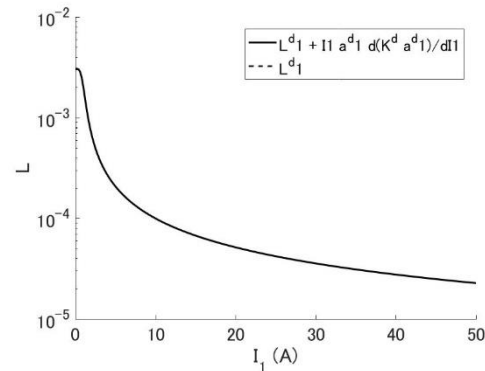
Figure 9. Result of $L_1^d + I_1 \left(\boldsymbol{a}_1^d\right)^{\mathrm{T}} \mathrm{d}\left(\boldsymbol{K}^d \boldsymbol{a}_1^d\right)/\mathrm{d}I_1$ using v^d is plotted in solid line.

4.2 Solution of State Equations

The output current is calculated with the help of state equations, which are solved with the prepared parameters.

A sinusoidal voltage E_S with an amplitude of 0.3 V and frequency $f = 5$ Hz is applied to the coil. When $B = 0$ and $f = 5$ Hz, the skin depth is approximately 2.3 mm. We chose the frequency at which the skin depth was smaller than the thickness of the iron core (5 mm) to observe the effect of eddy-current generation. The CLN used in the simulation consisted of five stages and was terminated with L_9. We also conducted a nonlinear transient analysis using the ordinary FEM.

The resultant total current I_t (in figure 1) obtained with the reluctivity v are shown in figure 10. The dots show the FEM results, while lines are obtained by applying the CLN method. The dotted line (linear) is the result of the linear CLN, which is far from the FEM result, as well as the dashed line (nonlinear 1) obtained by the nonlinear CLN neglecting the parameter variation terms. Both are calculated by solving the approximated state equations (16), (20), and (21). In contrast, the solid line (nonlinear 2) obtained from the parameterized CLN, including the parameter variation terms calculated by equations (16), (18), and (19), is close to the FEM result.

Figure 11 shows the results of the total current I_t when the reluctivity v^d is used. The solid line (nonlinear d), which is calculated from the nonlinear CLN by excluding the variation terms, is in good agreement with the FEM result. This fact indicates that the parameter variation terms can be neglected.
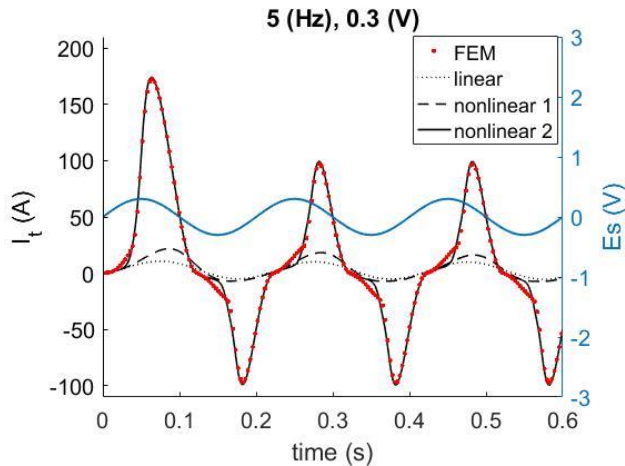
Figure 10. Transient waveform of the total current I_t obtained by the FEM and the CLN method when v is used with $\alpha = I_1$. The applied voltage E_S is shown in blue solid line.
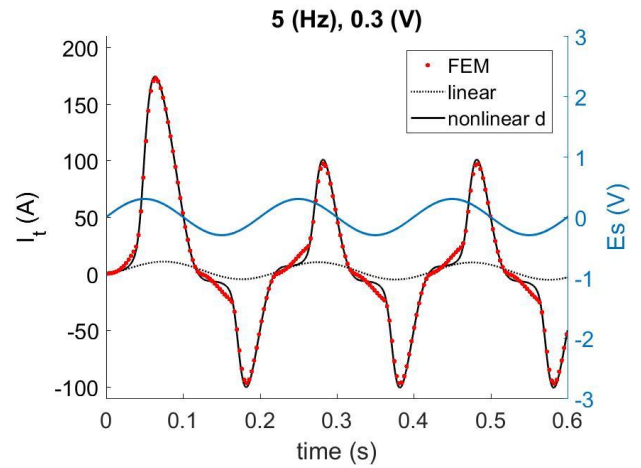

Figure 11. Transient waveform of the total current I_t obtained by the FEM and the CLN method when v^d is used with $\alpha = I_1$. The applied voltage E_S is shown in blue solid line.

Figure 12 shows the current I_{2n+1} ($n = 0, 1, 2$) flowing through each inductor L_{2n+1} for (a) nonlinear 1 and (b) nonlinear 2 based on the reluctivity v. The current I_1, which flows through the first inductor L_1, is the most dominant component in nonlinear 2, and it yields a result similar to that of the FEM. Currents I_3 and I_5 appear especially when the total current is less than approximately 50 A. The first-order approximation is not fully satisfied in that region, and thus, the current does not agree very accurately with the FEM result for low current. It should be noted that the applied frequency is not suitable for the bulk-type iron core, as mentioned before; hence, the first-order approximation is affected owing to the generation of the eddy-current field.

To improve the representation accuracy in the low current region, we can (a) parameterize not only with I_1 but also with I_3, or (b) use the total current I_t ($=\Sigma_n I_{2n+1}$) instead of I_1 as the parameter α when solving the state equations. The second method appeared to be effective in the study by Eskandari and Matsuo (2020).

When the differential reluctivity v^d is used, the current I_{2n+1} ($n = 0, 1, 2$) flowing through each inductor L_{2n+1}^d is shown in figure 13 for nonlinear d. The current I_1 is dominant in the high current region, indicating the validity of using the first-order approximation.
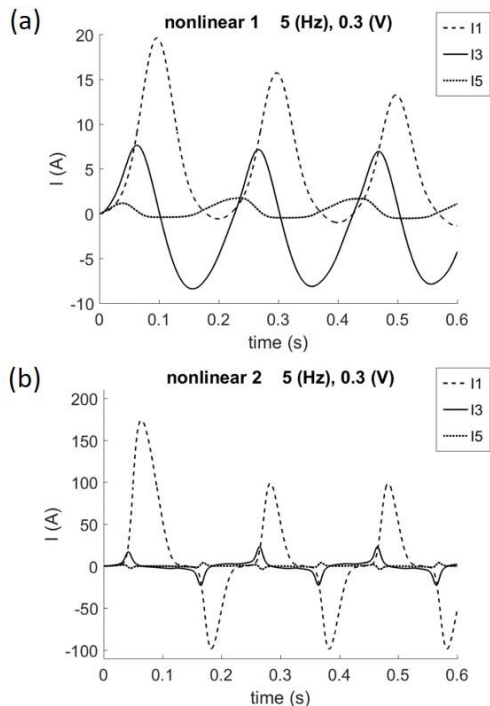
Figure 12. Computational results of each current for (a) nonlinear 1 and (b) nonlinear 2 in the CLN calculation when v is used.
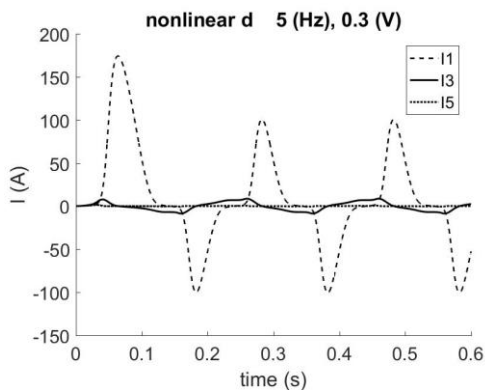
Figure 13. Each current for nonlinear d in the CLN calculation when v^d is used.

4.3 Computation Time

The computation time for the FEM and parameterized CLN is dominated by the solutions of the linear systems. The Newton–Raphson method was used for the nonlinear solutions, and it required approximately four iterations on average for convergence in both the FE analysis and the CLN method above.

Accordingly, the number of linear solutions required for the time-dependent nonlinear FE simulation is (the number of time steps) $\times 4$.

The CLN method, on the other hand, can yield any output under any transient input by solving the state equations, provided the network elements are prepared by the solutions beforehand. The CLN used in the simulation consists of five stages, and the preparation requires one nonlinear solution for the first stage to obtain L_1, and four linear solutions for the remaining stages ($L_3 - L_9$) per parameter. The number of linear solutions for the preparation was approximately (the number of parameters α) $\times 8$. The computational cost for solving the network equations is negligible. Therefore, the parameterized CLN

is faster than the FEM when (the number of time steps) > (the number of parameters α) $\times 2$ is satisfied.

The parameterized CLN significantly reduces the computation time, especially when (a) large time steps are required, for instance, PWM input and transient input for a long duration, and (b) calculations are conducted under various frequencies and voltages.

5. CONCLUSIONS

In this study, we formulated a parameterized CLN method to handle magnetic saturation, where the dynamic behavior of an orthogonal basis is represented by the parameter variation terms. The terms were newly derived by an exact formulation of the parameterized CLN.

The parameter variation terms play a significant role in the state equations when the reluctivity v is used, whereas they can be neglected when the differential reluctivity v^d is used. The computation time of nonlinear transient analyses can be greatly reduced by applying the parameterized CLN when the number of time steps is large.

In the future, we plan to extend the parameterized CLN to a multi-input multi-output to handle induction motors.

6. ACKNOWLEDGMENT

REFERENCES

Eskandari, H. and Matsuo, T. (2020), "Cauer Ladder Network Representation of a Nonlinear Eddy-current Field using a First-order Approximation," *IEEE Transactions on Magnetics*, Vol. 56, No. 2, p. 7505904.

Hasan, R. *et al.* (2018), "Stabilized reduced order model of a non-linear eddy current problem by a gappy-POD approach," *IEEE Transactions on Magnetics*, Vol. 54, No. 12, p. 8001808.

Henneron, T. and Clenet, S. (2014), "Model order reduction applied to the numerical study of electrical motor based on POD method taking into account rotation movement," *International Journal of Numerical Modelling*, Vol. 27, pp. 485–494.

Kameari, A. *et al.* (2017), "Cauer ladder network representation of eddy-current fields for model order reduction using finite element method," *IEEE Transactions on Magnetics*, Vol. 54, No. 3, p. 7201804.

Matsuo, T. *et al.* (2018), "Matrix formulation of the Cauer ladder network method for efficient eddy-current analysis," *IEEE Transactions on Magnetics*, Vol. 54, p. 7205805.

Sato, Y. *et al.* (2017), "Synthesis of Cauer-equivalent circuit based on model order reduction considering nonlinear magnetic property," *IEEE Transactions on Magnetics*, Vol. 53, No. 6, p. 1100204.

Shimotani, T. *et al.* (2016), "Fast finite-element analysis of motors using block model order reduction," *IEEE Transactions on Magnetics*, Vol. 52, No. 3, p. 7207004.

Tobita, M. and Matsuo, T. (2020), "Parameterized model order reduction and its application to nonlinear eddy-current field analysis," Abstract presented at Intermag 2020 Digest Book, CU-03, available at: https://intermag2020.com/storage/app/media/docs/Intermag20_Digests_Indx_1.pdf (accessed 12 January 2021).